Electronic Structure Studies of the Adenosylcobalamin Cofactor in Glutamate Mutase†

Amanda J. Brooks,‡ Christel C. Fox,§ E. Neil G. Marsh,§ Monica Vlasie,|| Ruma Banerjee,|| and Thomas C. Brunold*,‡

Department of Chemistry, University of Wisconsin−Madison, Madison, Wisconsin 53706, Department of Chemistry, University of Michigan, Ann Arbor, Michigan 48109, and Department of Biochemistry, University of Nebraska, Lincoln, Nebraska 68588

Received June 8, 2005; Revised Manuscript Received August 22, 2005

ABSTRACT: Glutamate mutase (GM) is a cobalamin-dependent enzyme that catalyzes the reversible interconversion of L-glutamate and L-threo-3-methylaspartate via a radical-based mechanism. To initiate catalysis, the 5′-deoxyadenosylcobalamin (AdoCbl) cofactor's Co−C bond is cleaved homolytically to generate an adenosyl radical and Co^{2+}Cbl. In this work, we employed a combination of spectroscopic and computational tools to evaluate possible mechanisms by which the Co−C bond is activated for homolysis. Minimal perturbations to the electronic absorption (Abs), circular dichroism (CD), and magnetic CD (MCD) spectra of AdoCbl are observed upon formation of holoenzyme, even in the presence of substrate (or a substrate analogue), indicating that destabilization of the Co^{3+}Cbl "ground state" is an unlikely mechanism for Co−C bond activation. In contrast, striking alterations are observed in the spectroscopic data of the post-homolysis product Co^{2+}Cbl when bound to glutamate mutase in the presence of substrate (or a substrate analogue) as compared to unbound Co^{2+}Cbl. These enzymatic perturbations appear to most strongly affect the metal-to-ligand charge-transfer transitions of Co^{2+}Cbl, suggesting that the cofactor/active-site interactions give rise to a fairly uniform stabilization of the Co 3d orbitals. Remarkable similarities between the results obtained in this study and those reported previously for the related Cbl-dependent isomerase methylmalonyl-CoA mutase indicate that a common mechanism by which the cofactor's Co−C bond is activated for homolytic cleavage may be operative for all base-off/His-on Cbl-dependent isomerases.

Glutamate mutase (GM)[1] belongs to a class of cobalamin-dependent enzymes that catalyze unusual carbon skeleton rearrangement reactions as shown in Figure 1A, where a substituent group on one carbon atom is exchanged with an H atom on an adjacent carbon atom (*1*−*6*). Specifically, GM catalyzes the reversible interconversion of L-glutamate and L-threo-3-methylaspartate (Figure 1B) as the first step in the fermentation pathway of glutamate in some *Clostridia* (*7*). The 5′-deoxyadenosylcobalamin (AdoCbl) cofactor (Figure 2) is essential to the catalytic cycle, initiating turnover through Co−C bond homolysis to generate Co^{2+}Cbl and an adenosyl (Ado·) radical. The adenosyl radical then proceeds to abstract an H atom from the substrate as the first step in the enzyme-mediated rearrangement reaction. Because of the unique sp^3 hybridization of the carbon-based migrating group

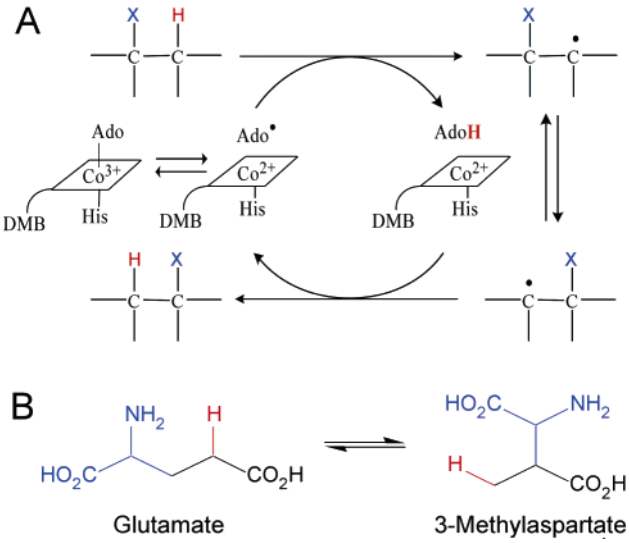

FIGURE 1: Generic mechanism for the AdoCbl-dependent isomerases (A) and the specific reaction catalyzed by GM (B), where glutamate undergoes a reversible 1,2-exchange reaction of the −H and $-C(CO_2H)(NH_2)$ groups, highlighted in red and blue, respectively, to produce 3-methylaspartate.

† Financial support was provided by the NSF (CAREER Grant MCB-0238530) to T.C.B. and the NIH (GM59227) to E.N.G.M. and (DK45776) to R.B. A.J.B. was supported by the NIH Training Grant in Molecular Biophysics (T32 GM08293).

* To whom correspondence should be addressed. 1101 University Avenue, Madison, WI 53706. Telephone: (608) 265-9056. Fax: (608) 262-6143. E-mail: brunold@chem.wisc.edu.

‡ University of Wisconsin−Madison.

§ University of Michigan.

|| University of Nebraska.

[1] Abbreviations: Abs, electronic absorption; ADF, Amsterdam density functional; AdoCbl, 5′-deoxyadenosylcobalamin; Cbl, cobalamin; CD, circular dichroism; CNCbl, cyanocobalamin; DFT, density functional theory; DMB, dimethylbenzimidazole; EPR, electron paramagnetic resonance; EXAFS, extended X-ray absorption fine structure; FTIR, Fourier transform infrared; Glu, L-glutamate; GM, glutamate mutase; HG, L-hydroxyglutarate; HOMO, highest occupied molecular orbital; LF, ligand field; LUMO, lowest unoccupied molecular orbital; MA, L-threo-3-methylaspartate; MCD, magnetic CD; MeCbl, methylcobalamin; MG, 2-methyleneglutarate; MLCT, metal-to-ligand charge transfer; MMCM, methylmalonyl-CoA mutase; MO, molecular orbital; rR, resonance Raman; TD-DFT, time-dependent DFT.

10.1021/bi051094y CCC: $30.25
Published on Web 10/29/2005

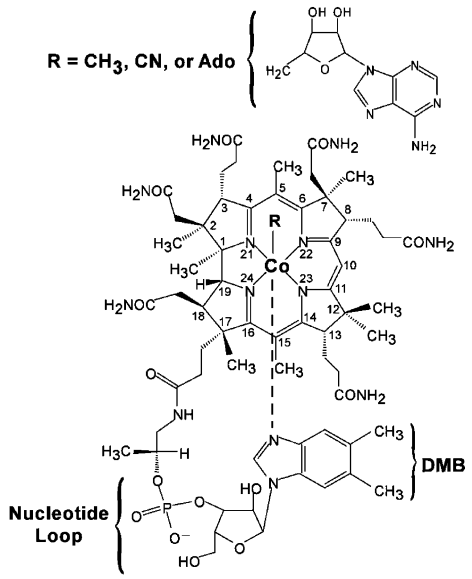

FIGURE 2: Schematic drawing of the free Cbl cofactor along with the standard atom numbering scheme used for the macrocycle. Note that when the cofactor binds to the GM active site, the intramolecular DMB is replaced by a protein-derived His residue.

of GM substrates, the rearrangement step is thought to proceed through an unusual fragmentation pathway (*8*−*11*). Reabstraction of the H atom from the adenosyl moiety and subsequent reformation of the cofactor's Co−C bond completes the catalytic cycle.

Interestingly, the Co−C bond of the free AdoCbl cofactor is quite strong, having an experimentally determined bond-dissociation energy in aqueous solution of ~32 kcal/mol (*12*). However, when AdoCbl is incorporated into the GM active site and substrate is added, a 10^{12}-fold rate acceleration is observed for homolytic cleavage of the cofactor's Co−C bond (*13*). Despite significant research efforts, the origin of this spectacular rate enhancement of Co−C bond cleavage, observed for all Cbl-dependent isomerases, remains one of the least well-understood aspects of enzymatic B_{12} chemistry. The two possible pathways by which GM can catalyze this rate enhancement are (a) weakening of the Co−C bond in the Co^{3+}Cbl "ground state" of the cofactor and/or (b) enzymatic stabilization of the post-homolysis products Co^{2+}-Cbl and Ado· or, in the case of a concerted or kinetically coupled mechanism, the substrate radical.[2]

Early structural and spectroscopic studies of free corrinoids and of holo-GM seemingly provided evidence in support of the ground-state destabilization theory. Upon cofactor binding, GM, like several other B_{12}-dependent enzymes, induces a ligand switch at the lower axial position, replacing the intramolecular dimethylbenzimidazole (DMB) with a protein-derived His residue (*14*, *15*). X-ray crystallographic studies have suggested that this ligand switch is accompanied by a significant increase in the Co−N_{ax} bond length; e.g., for methylcobalamin (MeCbl), Co−N_{ax} is 2.35 Å in the enzyme active site versus 2.16 Å in aqueous solution (*14*). Interestingly, a survey of a number of different cobalamin (Cbl) and cobaloxime species revealed that complexes possessing large Co−N_{ax} bond lengths also tend to have long Co−C bonds and vice versa, hinting toward the existence of an inverse trans influence (*16*). When these results are taken together, they might suggest that the Co−C bond is weakened upon binding to the enzyme, thus lending credence to the theory of ground-state destabilization. However, extended X-ray absorption fine structure (EXAFS) data indicated that the long Co−N_{ax} bond length observed crystallographically is likely an artifact of crystallization and/or X-ray structural data collection (*17*) and a more recent X-ray structure of GM complexed with AdoCbl and substrates revealed a "normal" Co−N_{ax} bond length of 2.2 Å (*18*). Additionally, resonance Raman (rR) spectra of the free and GM-bound AdoCbl cofactor have shown a shift in the Co−C stretching frequency of less than 2 cm^{-1}, indicating that the Co−C bond is not actually weakened in the enzyme active site to any significant degree (*19*). Overall, evidence in support of the ground-state destabilization hypothesis appears to be inconclusive at best.

Lowering the activation barrier for homolytic cleavage of the cofactor's Co−C bond via stabilization of the post-homolysis products has been proposed by numerous research groups and is the prevailing model invoked to rationalize the rate acceleration for Co−C bond homolysis for a variety of AdoCbl-dependent enzymes, including ribonucleotide reductase (*20*) and methylmalonyl-CoA mutase (MMCM) (*21*, *22*). To date, spectroscopic studies of Co^{2+}Cbl bound to the GM active site have been limited primarily to electronic absorption (Abs) and electron paramagnetic resonance (EPR) experiments. Unfortunately, the transient nature of the Co^{2+}Cbl form of the cofactor and inherent presence of a mixture of AdoCbl and Co^{2+}Cbl under turnover conditions has greatly limited the information gained from Abs spectroscopy. Although EPR spectroscopy overcomes these limitations because of its selectivity for paramagnetic species, the localization of the unpaired electron of Co^{2+}-Cbl in a Co 3d-based molecular orbital (MO) that has little contribution from the equatorial nitrogens (*23*) largely limits the sensitivity of the technique to only axial perturbations of the cofactor. Therefore, despite advances made in elucidating the geometric and electronic properties of the enzyme-bound reduced cofactor, the current understanding of the Co^{2+}Cbl/GM active-site interactions is still fairly limited.

We have previously demonstrated the power of our combined spectroscopic/computational approach to gain molecular-level insight into changes in the electronic structure and thus the reactivity of the AdoCbl cofactor when it binds to the MMCM active site (*22*, *24*). In an effort to assess whether the Co−C bond activation mechanism proposed for MMCM also applies to other B_{12}-dependent isomerases, we present here a parallel study of the cofactor/active-site interactions for GM. Electronic Abs, circular dichroism (CD), and magnetic CD (MCD) spectroscopic results are presented and interpreted within the framework of density functional theory (DFT) and time-dependent DFT (TD-DFT) for both the AdoCbl cofactor and its post-homolysis product Co^{2+}Cbl bound to the GM active site in the absence and

[2] According to Hammond's postulate, the radical species generated in a homolytic cleavage reaction would be very close in energy to the transition state. In such a case, stabilization of the products will consequently also lower the energy of the transition state, reducing the activation barrier and increasing the rate of homolytic Co−C bond cleavage.

presence of substrate (or a substrate analogue).[3] Complementary spectroscopic data obtained for the AdoCbl derivatives MeCbl and cyanocobalamin (CNCbl) are used as the basis for further evaluation of cofactor/active-site interactions through the development of spectro/structural correlations, whereby the effects of axial distortions on the spectroscopic and electronic properties of these cofactors are systematically explored. Together, these studies provide significant, new qualitative insight into the geometric and electronic factors contributing to the dramatic acceleration of Co−C bond homolysis accomplished by GM.

MATERIALS AND METHODS

Materials. AdoCbl, MeCbl, CNCbl, L-glutamic acid (Glu), L-α-hydroxyglutaric acid (HG), and DL-*threo*-*β*-methylaspartic acid (MA) were purchased from Sigma and used as obtained without further purification. The substrate analogue 2-methyleneglutarate (MG) was synthesized as described previously (*25*). The L-α-hydroxyglutaric acid and 2-methyleneglutarate solids were dissolved in 1 M NaOH to a final concentration of 0.5 M, while the L-glutamic acid and DL-*threo*-*β*-methylaspartic acid solids were dissolved in 1 M NaOH to a final concentration of 1 M to generate the sodium salts. These stock solutions were then diluted to 50 mM using 50 mM potassium phosphate buffer at pH 7. Co^{2+}Cbl was generated by reduction of H_2OCbl^+ using the flavin system from *Salmonella enterica* as described previously (*26*, *27*).

Purification of GM. The GM fusion protein GlmES was purified from a recombinant *Escherichia coli* strain as previously described by Chen and Marsh (*28*) with modifications described by Cheng (*29*). Reconstitution of GlmES with the AdoCbl, MeCbl, and CNCbl cofactors was carried out in the dark at 4 °C.

Sample Preparation. Samples of the free cofactors and holo-GM (reconstituted with AdoCbl, MeCbl, or CNCbl) were prepared in 60% (v/v) glycerol glassing agent to ensure glass formation upon freezing. Each sample was purged with Ar gas for 15 min, injected into an MCD sample cell and then immediately frozen in liquid N_2. Protein samples containing substrate (analogues) were prepared by the addition of an appropriate aliquot of the corresponding stock solution to an Ar-purged solution of holoenzyme in 60% (v/v) glycerol glassing agent. For the AdoCbl/GM and MeCbl/GM samples, an approximately 25-fold molar excess of substrate was added except for methylaspartate, which was added in a 5-fold molar excess. A greater than 45-fold molar excess of each substrate was added to the CNCbl/GM samples. With substrate K_d values ranging from 37 μM for methylaspartate (*13*) to 3 mM for 2-hydroxyglutarate (*30*), these ratios ensured complete conversion to the substrate-bound forms of the holoenzyme. Protein concentrations ranged from 0.17 mM (CNCbl/GM) to 0.49 mM (AdoCbl/GM and MeCbl/GM) and were determined spectrophotometrically at 300 K on the basis of published molar extinction coefficients ($\epsilon_{522} = 8000\ M^{-1}\ cm^{-1}$ for AdoCbl, $\epsilon_{528} = 7900\ M^{-1}\ cm^{-1}$ for MeCbl, and $\epsilon_{551} = 8740\ M^{-1}\ cm^{-1}$ for CNCbl (*31*)). Samples were frozen within 1 min of substrate (analogue) addition. All samples were handled under reduced light to prevent undesired photolysis of the cofactors' Co−C bond. After data collection for the GM samples reconstituted with AdoCbl and MeCbl, each sample was thawed at room temperature in the dark and then exposed to room light for up to 2 h. Conversion to the Co^{2+}Cbl state through photolysis was followed by monitoring the loss and gain of Abs intensity at 525 and 474 nm, respectively. After an adequate level of conversion (∼30−60%) to the Co^{2+}Cbl state was reached, the samples were refrozen in liquid N_2. All attempts to photolyze the CNCbl/GM samples with and without substrate (or a substrate analogue) present were unsuccessful, as expected on the basis of the high resistivity of CNCbl toward photolysis.

Spectroscopy. Room-temperature Abs spectra were recorded on a Varian Cary 5e spectrophotometer. Low-temperature Abs, CD, and MCD spectra were collected using a Jasco J-715 spectropolarimeter in conjunction with an Oxford Instruments SM-4000 8T magnetocryostat. MCD spectra of GM samples reconstituted with AdoCbl and MeCbl were collected at a range of temperatures including 4.5, 10, 25, 50, and 150 K. Abs, CD, and MCD spectra of GM reconstituted with CNCbl were collected on fluid samples at 250 K to prevent baseline distortions arising from glass strain. All MCD spectra shown in this paper were obtained by subtracting the −7 T spectrum from the +7 T spectrum to eliminate contributions from the natural CD.

Fourier transform infrared (FTIR) spectra of free and GM-bound CNCbl were collected on a Mattson Galaxy Series FTIR 7000 spectrometer at ambient temperature. For each sample, a 10 μL aliquot was suspended between two CaF_2 windows separated by a 56 μm Teflon spacer. The sample compartment was purged with N_2 for 2.5 min prior to data collection, and deionized water was used as a reference spectrum. The vibrational feature associated with the C≡N stretching mode was fit with a Gaussian band to determine the exact position of the peak maximum using the curve fitting macro provided in the Igor Pro 3.14 software package.

Computational Models. The models used for DFT calculations on CNCbl were based on coordinates from synchrotron data collected at 100 K (CSD code WIKXUJ) (*32*). All corrin ring substituents, including the nucleotide loop, were replaced with H atoms at 1.08 Å from the neighboring C atoms, and the DMB base was modeled as an imidazole while preserving the original Co−N_{ax} bond distance and orientation. This truncation scheme has been used previously for Co^{3+}- and Co^{2+}-corrinoid species and was shown to preserve all essential electronic features of the full corrinoids (*23*, *33*). To generate CNCbl models with varying axial bond lengths for the spectro/structural correlations, the positions of all atoms of one axial ligand were optimized as a function of the trans axial ligand bond length, which was systematically altered in increments of 0.1 Å. The coordinates of all atoms of the corrin macrocycle were kept frozen during these optimizations to preserve the crystallographic conformation of the corrin, because the truncation scheme employed here

[3] Although enzymatic stabilization of the other post-homolysis product, the Ado· radical, may also contribute to the rate acceleration for Co−C bond cleavage, this possibility cannot be explored with the spectroscopic techniques employed in this study. However, we have previously shown that 5′-deoxyadenosine, which differs from the Ado· radical by only a single hydrogen atom, is merely a weak-binding competitive inhibitor of the enzyme ($K_i \approx 2$ mM, see ref *27*). This observation argues against the Ado· radical/protein interaction, playing a large role in promoting Co−C bond homolysis, because otherwise we would expect 5′-deoxyadenosine to be a more potent inhibitor of the enzyme.

removes certain structural constraints that are known to influence corrin folding (*34*, *35*).

All geometry optimizations were carried out on an ACE computer cluster equipped with 20 Intel Xeon processors using the Amsterdam Density Functional (ADF) 2003.01 suite of programs (*36*−*38*). Each optimization was performed with an integration constant of 4.0 and the Vosko−Wilk−Nusair local density approximation (*39*) with the nonlocal gradient corrections of Becke (*40*) for exchange and Perdew (*41*) for correlation. ADF basis set IV was chosen for all atoms with core orbitals frozen through 1s for C, N, and O and 2p for Co. The SCF convergence criterion was set at 1×10^{-6} hartrees, and the geometry was considered converged when the maximum gradient fell below 0.005 hartrees. The geometry-optimized atomic coordinates for all models mentioned in the text are provided in the Supporting Information (Tables S1−S22).

Single-Point DFT Calculations. Single-point DFT calculations on all cofactor models were carried out using the ORCA 2.2 software package developed by Dr. Frank Neese (MPI Mülheim, Germany) (*42*). The Ahlrichs polarized split valence [SV(P)] basis (*42*, *43*) along with the SV/C auxiliary basis (*45*) were used for all atoms with the exception of Co, which was treated with the larger TZVP (triple-ζ valence polarization) basis (*44*, *45*). In each case, Becke's three parameter hybrid functional for exchange (*47*, *48*) combined with the Lee−Yang−Parr correlation functional (*49*) (B3LYP/G) were employed, a combination shown previously to yield particularly good agreement between experimental and computed electronic structure descriptions of Co^{3+} corrinoids (*32*). The default SCF convergence criterion of 1×10^{-6} hartrees and an integration grid size of 3 (Lebedev 194 points) were used for all calculations.

TD-DFT Calculations. The TD-DFT method (*50*−*52*) within the Tamm−Dancoff approximation (*53*, *54*) as implemented in ORCA 2.2 was used to calculate transition dipole moments and vertical excitation energies for all ADF geometry-optimized models employing the same hybrid functional and basis sets described above for the single-point DFT calculations. The resolution of the identity approximation (*55*) was used to evaluate the Coulomb term to improve the computational efficiency of the TD-DFT calculations. A total of 40 excited states were calculated for each model by including all one-electron excitations within ±3 hartrees of the highest occupied molecular orbital (HOMO)/lowest unoccupied molecular orbital (LUMO) energies. All spectra were red-shifted by 5500 cm^{-1} to compensate for the fact that transition energies for Co^{3+}-corrinoids are consistently overestimated by the B3LYP TD-DFT method (*23*, *32*, *51*, *55*).

RESULTS AND ANALYSIS

AdoCbl and MeCbl Spectroscopy: Resting States. Comparisons of the low-temperature Abs, CD, and MCD spectra of the free and GM-bound cofactors are shown in Figure 3 for AdoCbl (R state, top) and MeCbl (R′ state, bottom).[4] In these studies, the AdoCbl derivative MeCbl was used as a means to assess the importance of direct interactions between

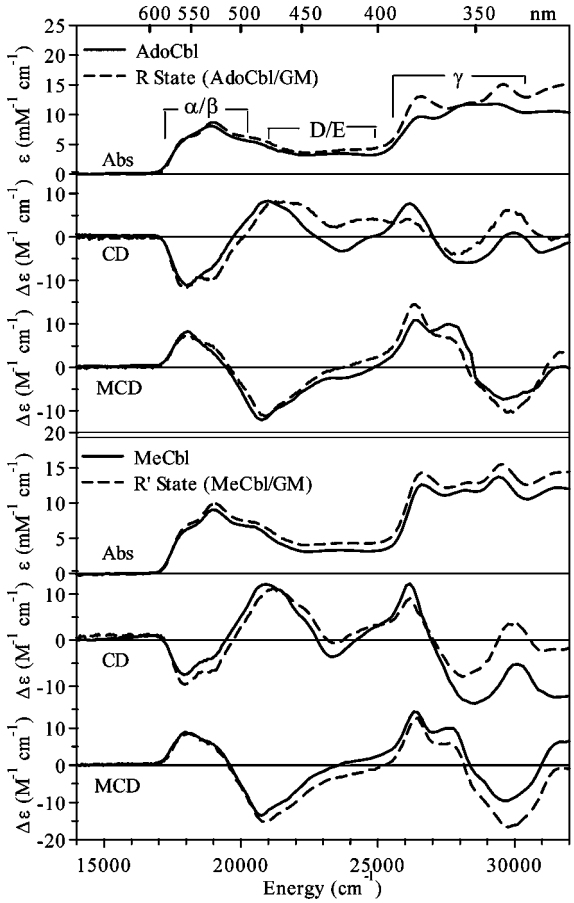

FIGURE 3: Abs (4.5 K), CD, and 25 K 7 T MCD spectra of free and GM-bound AdoCbl (top) and MeCbl (bottom). Band designations are given above the AdoCbl Abs spectra.

the bulky Ado moiety and the enzyme active site with respect to the Co−C bond activation mechanism. The Abs spectra of the free cofactors, as well as of the R state, agree well with those reported in the literature (*19*, *31*, *57*), indicating that the addition of glycerol and the cryogenic temperatures used in this study did not perturb the cofactor to any significant degree. Detailed assignments of all features in the Abs spectra of the free cofactors have been reported previously (*33*) and will not be discussed in detail here.

Qualitatively, the Abs, CD, and MCD spectra of the free cofactors and their GM-bound forms are extremely similar with respect to band positions and intensities, revealing only minor perturbations of the cofactors' electronic structures by the enzyme active site. Most notably, holoenzyme formation results in a modest increase in Abs intensity for both AdoCbl and MeCbl. This phenomenon can be attributed to the altered dielectric environment of the cofactor in the enzyme active site compared to aqueous solution; similar changes have been observed previously for the AdoCbl-dependent isomerase MMCM (*58*). Interestingly, this effect is less dramatic for GM than for MMCM, suggesting that the GM active site is less hydrophobic and thus more solvent-exposd than the MMCM active site. This hypothesis is consistent with the fact that the Cbl-binding site of GM lies at the interface of two subunits, whereas that of MMCM is buried inside a single protein subunit. A second notable feature of the spectroscopic data in Figure 3 is the increased band resolution in the R state spectra compared to the free AdoCbl spectra, suggesting that the cofactor is forced to

[4] The MCD spectra of both the free and GM-bound cofactors were found to be temperature-independent (data not shown), consistent with the diamagnetic nature of the cofactors in their Co^{3+} state.

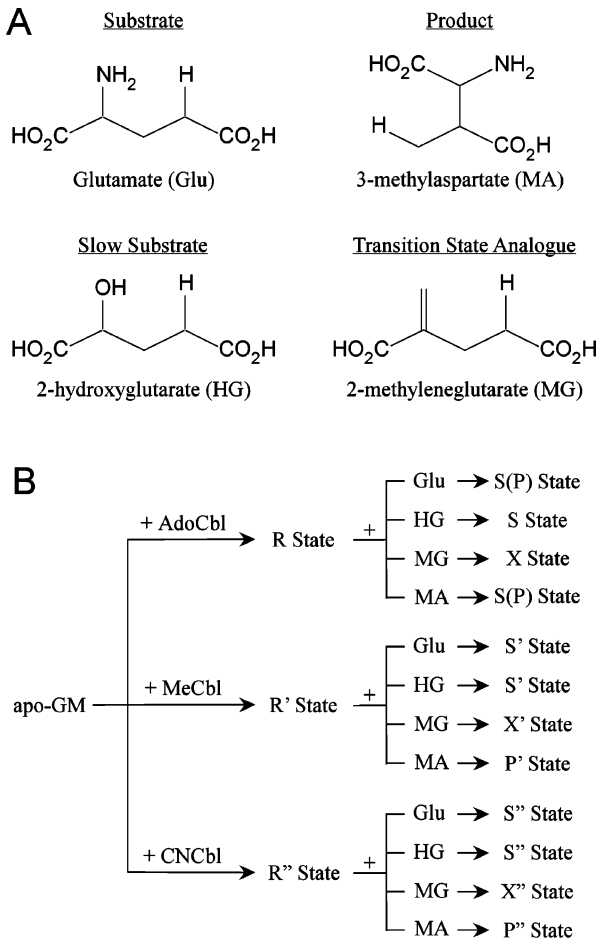

FIGURE 4: (A) Schematic structures for the native substrate Glu, the product MA, the slow substrate analogue HG, and the mechanism-based inhibitor MG. (B) Nomenclature used for the samples studied in this work. Note that the addition of the actual substrate (glutamate) and product (3-methylaspartate) to GM-bound AdoCbl (R state) yields a mixture of the substrate- and product-bound states in a 12:1 ratio (*13*).

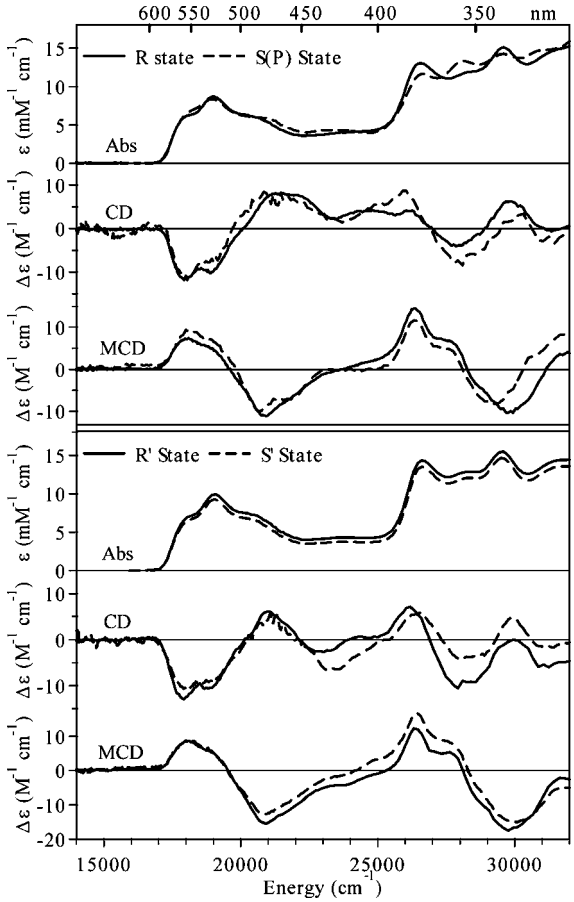

FIGURE 5: Abs (4.5 K), CD (4.5 K), and 7 T MCD (25 K) spectra of GM-bound AdoCbl (top) and MeCbl (bottom) in the absence (R/R′ state) and presence [S(P)/S′ state] of the native substrate, glutamate.

adopt a more defined conformation in the GM active site, presumably through stabilization of a fixed orientation of the adenosyl moiety above the corrin plane. Support for this model is provided by published rR spectra of holo-GM, which revealed a dramatic increase in the relative intensity of one of two Co−C stretching modes observed for free AdoCbl that are attributed to different conformations of the Ado moiety with respect to the corrin ring (*19*). Again, a similar effect has been noted previously for MMCM (*24*, *59*−*61*). In contrast, the Abs, CD, and MCD spectra of MeCbl do not change significantly upon cofactor binding to GM and are almost identical to those of GM-bound AdoCbl. This result is expected because the only conformational freedom of the upper axial ligand of MeCbl involves rotation of the methyl group about the Co−C bond vector, which is not expected to affect the electronic structure and thus spectroscopic data of MeCbl.

Substrate (Analogue) States. To probe the electronic structures of the AdoCbl and MeCbl cofactors bound to GM in the substrate-bound (S/S′) state, inhibitor-bound (X/X′) state, and product-bound (P/P′) state (Figure 4), the natural substrate, Glu, and product, MA, were utilized, along with the slow substrate HG and the mechanism-based inhibitor MG. The addition of the substrate (analogues) to apo-GM reconstituted with AdoCbl induced rapid Co−C bond cleavage, resulting in the formation of a small percentage of paramagnetic Co^{2+}Cbl before the samples could be frozen. Importantly, however, the $1/T$ dependence of the contributions from this species to the MCD signal allowed us to resolve the spectral features arising solely from the Co^{3+}-Cbl form of the cofactors by collecting data at elevated temperatures (150 K). In contrast, incubation of the MeCbl/GM complex with substrate (analogues) in the dark did not induce Co−C bond cleavage, providing an alternative means of probing the S-, X- and P-like states (termed S′, X′, and P′, respectively) without any Co^{2+}Cbl contributions (Figure 4).

Figure 5 compares the Abs and MCD spectra of the R/R′ state with those of the S(P)/S′ state generated using the native substrate glutamate (Figure 4B), allowing the effects of substrate binding to holo-GM on the cofactors' geometric and electronic properties to be assessed. Note that turnover occurred when holo-GM samples were mixed with glutamate and methylaspartate, resulting in these samples being a mixture of the S and P states in a 12:1 ratio (Figure 4B) (*13*). Importantly, the Abs, CD, and MCD spectra of apo-GM reconstituted with a given cofactor are all virtually identical regardless of the substrate (analogue) used (see Figure S1 in the Supporting Information), suggesting that the electronic structure of the cofactor in the Co^{3+} ground state does not vary as a function of the specific substrate (analogue) added. Although small but notable differences

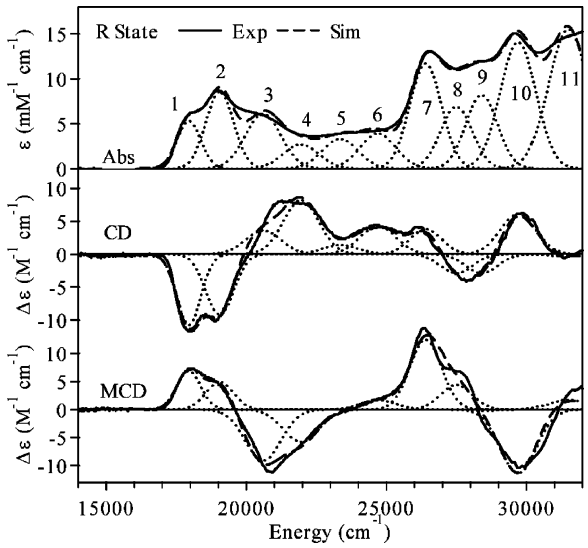

FIGURE 6: (—) 4.5 K Abs, CD, and 7 T MCD spectra of GM-bound AdoCbl. (•••) Gaussian deconvolutions of the experimental spectra obtained with the fit parameters provided in Table 1. (- - -) Sum of individual Gaussian bands.

exist between the R and S(P) state Abs and CD spectra (Figure 5, top), the band shifts and intensity changes near 21 000 and 28 000 cm^{-1} can be attributed to the presence of Co^{2+}Cbl in the S(P) state sample and thus do not reflect any significant alterations to the ground-state electronic structure of the cofactors.

AdoCbl and MeCbl Spectral Analysis. The Abs, CD, and MCD spectra discussed above were iteratively fit with the fewest possible number of Gaussian bands to determine the energies and intensities of the major electronic transitions. These spectroscopic parameters provide the necessary framework for a quantitative comparison of the holo-GM spectra in the absence and presence of substrate (or a substrate analogue) with those of the free cofactors. As a representative example, Gaussian deconvoluted Abs, CD, and MCD spectra of the AdoCbl/GM R state are shown in Figure 6. Band energies obtained from spectral fits of free AdoCbl and MeCbl as well as the R/R′ states and S(P)/S′ states generated using glutamate are listed in Table 1. Fit parameters for additional substrate analogue states are provided in the Supporting Information (see Table S23).

Resting States. Of the bands that contribute to the most intense and best resolved features in the Abs spectra of the free cofactors (bands 1−3 and 7−10, Figure 6), none are observed to shift more than 200 cm^{-1} upon cofactor binding to GM (Table 1). In fact, several bands exhibit shifts that fall within the range of estimated experimental error ($|\Delta| \leq$ 100 cm^{-1}). These results provide further evidence that binding of AdoCbl and MeCbl to the GM active site only minimally perturbs the electronic, and thus also the geometric, structures of the cofactors. To verify that these minor band shifts rule out larger changes to the cofactors' geometric and electronic properties, the data in Table 1 were analyzed within the framework of our previously developed spectro/structural correlations for MeCbl (*24*), where the effects of geometric perturbations of the cofactor on the corresponding Abs spectrum were evaluated using TD-DFT. Importantly, these previous studies revealed that band 1 is particularly sensitive to perturbations in the axial bonding scheme. Thus, the 80 cm^{-1} blue shift of band 1 between the spectra of free

Table 1: Fit Parameters Derived from Gaussian Deconvolutions of the Experimental Abs, CD, and MCD Spectra (for Example, see Figure 5) of the Free, Holo-GM, and Substrate-Bound GM Reconstituted with AdoCbl (Top) and MeCbl (Bottom)[a]

band	AdoCbl	R state	S(P) state (Glu)	Δ GM binding	Δ Glu binding
1	17 875	17 950	17 900	75	−50
2	18 925	19 050	19 000	125	−50
3	20 600	20 600	20 700	0	100
4	21 900	21 950	21 950	50	0
5	23 400	23 350	23 350	−50	0
6	24 800	24 700	24 850	−100	150
7	26 350	26 400	26 350	50	−50
8	27 600	27 500	27 575	−100	75
9	28 400	28 400	28 450	0	50
10	29 550	29 700	29 625	150	−75
11	31 400	31 500	31 250	100	−250

band	MeCbl	R′ state	S′ state (Glu)	Δ GM binding	Δ Glu binding
1	17 870	17 950	17 950	80	0
2	19 000	19 050	19 050	50	0
3	20 550	20 700	20 450	150	−250
4	21 900	21 900	21 700	0	−200
5	23 450	23 350	23 200	−100	−150
6	24 900	24 600	24 800	−300	200
7	26 500	26 400	26 500	−100	100
8	27 550	27 600	27 750	50	150
9	28 350	28 550	28 550	200	0
10	29 600	29 750	29 700	150	−50
11	31 600	31 500	31 500	−100	0

[a] All band positions and band shifts are given in cm^{-1} units.

and GM-bound MeCbl corresponds to only a 0.015 Å increase in the Co−N_{ax} bond length or a 0.012 Å decrease in the Co−C bond length. We favor the former scenario because (i) previous rR experiments revealed that the Co−C stretching frequency of AdoCbl is unaffected by cofactor-binding to apo-GM (*19*) and (ii) the amino acid side chains in the active site of GM are not expected to interact strongly with the methyl group of MeCbl because the enzyme evolved to accommodate the much bulkier adenosyl moiety. Because these estimates represent upper limits for the enzyme-induced axial perturbations of the cofactor,[5] the existence of an unusually long Co−N_{ax} bond in the active site seems highly unlikely. Most importantly, the lower axial ligand switch from the intramolecular DMB to His^{16} in the R/R′ state (*14*) does not appear to alter the electronic structure of the cofactor to any significant degree.

Because folding of the corrin macrocycle has frequently been proposed as a source of Co−C bond activation, structural perturbations involving this coordinate were also evaluated using our spectro/structural methodology. The position of band 9 has previously been shown to exhibit the greatest dependence on the corrin fold angle[6] (*24*). Using this band, the spectro/structural correlations predict a maximum fold angle increase of 10° based on the 200 cm^{-1} blue shift of band 9. Although distortions of the cofactor along this coordinate in the enzyme active site appear quite

[5] Because these bond length changes were estimated under the assumption that enzymatic perturbations of the cofactor involve a single structural coordinate, each value represents the maximum geometric distortion along that coordinate compatible with our spectroscopic data.

[6] The fold angle corresponds to the angle between the mean planes defined by the atoms N^{21}-C^4-C^5-C^6-N^{22}-C^9-C^{10} and C^{10}-C^{11}-N^{23}-C^{14}-C^{15}-C^{16}-N^{24}.

substantial, it is important to note that folding of the corrin macrocycle is not expected to alter the Co−C bond strength to any significant degree (*24*). In addition, rR studies revealed that the macrocycle stretching frequencies are insignificantly affected by binding of the cofactor to the GM active site (*19*), indicating that folding of the corrin macrocycle also has little effect on the electronic properties of the corrin ring.

Substrate (Analogue)-Bound States. Gaussian deconvolutions of the Abs, CD, and MCD spectra obtained for the substrate (analogue)-bound holo-GM samples reveal insignificant differences in the positions of a majority of the bands among the different data sets (Table S23 in the Supporting Information) as expected on the basis of their close resemblance. This quantitative analysis of the spectroscopic results also indicates that the Abs, CD, and MCD spectra of the substrate-bound MeCbl/GM samples are more similar to one another than are the spectra of the substrate-bound AdoCbl/GM samples. However, it is important to note that the presence of a small but varying percentage of Co^{2+}Cbl in the AdoCbl/GM S, P, and X state samples can account for the minor differences in apparent band positions. Consistent with our qualitative analysis presented above, a comparison of the band positions for the R/R′ and S(P)/S′ state spectra (Tables 1 and S23 in the Supporting Information) confirms that addition of Glu to holo-GM does not dramatically influence the electronic structures of the cofactors in their Co^{3+} ground states. Many of the observed band shifts are $\leq$100 cm^{-1} (and thus within the estimated experimental error), and even the largest shift is only 250 cm^{-1} (band 10 for the R → S/P state conversion and band 3 for the R′ → S′ state conversion). As evidenced by the spectro/structural correlations described above, band shifts of this magnitude correlate with only minor geometric changes, thus ruling out that the Co−C bonding interactions in the AdoCbl and MeCbl cofactors are perturbed in any substantial way by GM even in the presence of substrate (or a substrate analogue).

CNCbl Spectroscopy. While our studies of GM reconstituted with AdoCbl and MeCbl presented above have provided significant insight into the cofactor/active-site interactions and their effects on the Co−C bond properties, the alkyl groups of these cofactors are known to dominate the axial bonding scheme through strong Co−C σ-bonding interactions (*33*), possibly masking changes that are occurring at the trans Co−N_{ax} bond. Thus, to investigate the possibility of protein-induced modulation of the Co−N_{ax} bond with greater sensitivity, we sought a cofactor analogue that possessed an axial Co−C bond whose bonding interactions with Co would not completely dominate the axial bonding scheme. CNCbl, perhaps better known as vitamin B_{12}, seemed an ideal candidate because it has been well-characterized structurally and spectroscopically (*31*−*33*, *62*), CN^- is known to be a moderate σ-donor, and GM has previously been crystallized with CNCbl in the active site (*14*). Consequently, GM was reconstituted with CNCbl in the absence and presence of substrate (and substrate analogues) and examined using our spectroscopic techniques.

A comparison of the Abs, CD, and MCD spectra obtained for free and GM-bound CNCbl in the absence (R″ state) and presence (S″ state) of glutamate is provided in Figure 7. The free CNCbl Abs spectrum exhibits the spectral signatures characteristic of a "typical" Cbl cofactor, including a broad band at low energy displaying a partially resolved

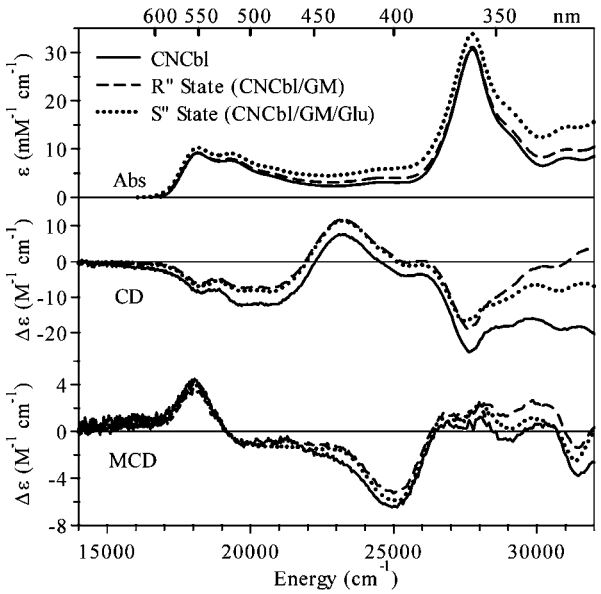

FIGURE 7: Abs, CD, and 7 T MCD spectra at 250 K of free CNCbl (—), GM-bound CNCbl (R″ state, - - -), and GM-bound CNCbl in the presence of glutamate (S″ state, ···).

vibrational progression (the α/β bands) and a more intense, sharper feature at higher energy (the γ band) (*31*, *33*). From Figure 7, it appears as though incorporation of CNCbl into the GM active site to generate the R″ state has virtually no effect on the corresponding Abs, CD, and MCD spectra. The increase in Abs intensity that is observed upon formation of the holoenzyme using AdoCbl and MeCbl is also observed here for CNCbl but to a much lesser extent. In fact, the overwhelming similarity of the free CNCbl and R″ state spectra raised questions as to whether the CNCbl cofactor was actually being incorporated into the GM active site under the conditions used in preparing our samples. To address this issue, FTIR spectra were collected for free and GM-bound CNCbl, because a change in the C≡N stretching frequency would be expected to occur in response to cofactor binding to the GM active site. Upon the addition of GM, a slight shift in the CN stretching frequency was observed from 2127 to 2131 cm^{-1} (Figure S2 in the Supporting Information), consistent with the enzyme-bound CNCbl cofactor being localized in an environment that has a dielectric constant lower than water. Considering that in the X-ray structure of CNCbl/GM the cyano group is surrounded by a hydrophobic protein pocket and thus protected from the solvent (*14*), this result can be interpreted as indicating that the CNCbl cofactor indeed binds to GM under the conditions used.

As noted above for AdoCbl and MeCbl, addition of substrate (or a substrate analogue) to holo-GM reconstituted with CNCbl does not appear to alter the electronic structure of the cofactor to any significant degree. Although only the spectra of the S″ state prepared with glutamate are presented in Figure 7, all of the substrate (analogue) states generated exhibit nearly identical Abs, CD, and MCD spectra (Figure S3 in the Supporting Information). Collectively, these results suggest that the GM-induced perturbations of the CNCbl cofactor are extremely minor, even in the presence of substrate (or a substrate analogue).

CNCbl Spectral Analysis. The Abs, CD, and MCD data sets for all samples containing CNCbl were iteratively fit

with a constant number of Gaussian bands to determine the energies and shifts of the major electronic transitions contributing to the visible/near-UV spectral region, as described above in the AdoCbl and MeCbl spectral analysis section. In light of the qualitative similarities that exist among these spectra, it is not surprising that our Gaussian deconvolutions reveal only insignificant band shifts between the various CNCbl states (Table S24 in the Supporting Information). All band positions deduced from the R″, S″, X″, and P″ state spectra are within ± 50 cm^{-1} of those found for free CNCbl, well within the range of the estimated experimental error.

CNCbl Spectro/Structural Correlations. Because the electronic spectra of Co^{3+}Cbls are dominated by $\pi \rightarrow \pi^*$ transitions localized on the corrin macrocycle (*33*), the absence of any significant band shifts in the experimental spectra (Figures 3 and 5 and Table 1) does not necessarily rule out protein-induced perturbations of the cofactor's axial Co−C and Co−N_{ax} bond in the Co^{3+} state. This is particularly true for CNCbl in which the axial Co−C bonding interactions are considerably weaker than those in alkylcobalamins (because of the much greater σ-donating ability of the alkyl groups than CN^-), reducing the ability of the axial ligands to effectively communicate via the Co 3d orbitals with the π/π^* frontier MOs of the corrin macrocycle. To explore the consequences of structural distortions on the electronic properties of CNCbl, we have extended our previously developed spectro/structural methodology (*24*) to predict how the electronic spectra of CNCbl would change upon specific alterations to the axial bonding scheme.

A series of partial geometry optimizations were performed starting from a CNCbl model based on crystal structure coordinates (see the Materials and Methods section), where the Co−C and Co−N_{ax} bond lengths were systematically varied up to ± 0.5 Å from their equilibrium distances of r(Co−C) = 1.88 Å and r(Co−N_{ax}) = 2.04 Å (*32*). For each set of bond lengths, one axial ligand was fixed at the desired distance, while the position of the trans axial ligand was allowed to optimize, keeping all atomic coordinates of the corrin macrocycle frozen. Relevant results from these calculations are presented in Figure 8 and Table S25 in the Supporting Information.

The structural correlations revealed by these partial geometry optimizations provide interesting insight into the nature of the axial bonding interactions in CNCbl. As the Co−C bond is stretched from 1.38 to 2.38 Å, the optimized Co−N_{ax} bond length decreases considerably from 2.28 to 2.01 Å, characteristic of a normal axial trans influence. Lengthening of the Co−N_{ax} bond from 1.54 to 2.54 Å has a similar, although less substantial, effect on the Co−C bond length, which decreases from 1.99 to 1.84 Å. From our previous studies of free Co^{3+}-corrinoids (*33*), σ donation of electron density from the upper axial ligand into the (empty) Co $3d_{z^2}$ orbital induces some Co−N_{ax} σ-antibonding character and thus modulates the Co−N_{ax} bond length. The moderate σ-donating character of the cyanide ligand means that although the Co−C bonding interaction will be strong (in part because of π back-bonding), the lower axial base, a similarly strong σ donor, also plays an important role in the axial bonding scheme. As a result, increasing either the Co−C or the Co−N_{ax} bond length and thus lowering the corresponding bond strength will lead to a stronger interaction (and thus a shorter bond) for the trans axial ligand. The CN^- ligand is still predicted by DFT to dominate the bonding scheme, however, modulating the Co−N_{ax} bond length almost twice as much as the lower axial imidazole ligand alters the Co−C bond length (Figure 8).

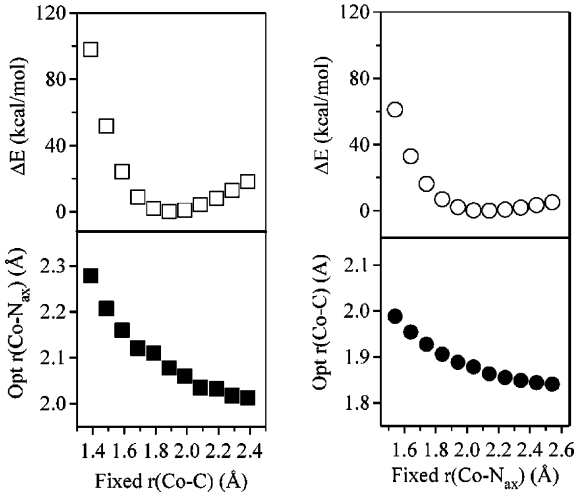

FIGURE 8: Calculated potential energy surfaces (top) and bond length correlations (bottom) for CNCbl, where the Co−C bond length (left) and Co−N_{ax} bond length (right) were systematically varied by ± 0.5 Å from their equilibrium distances of 1.88 and 2.04 Å, respectively.

Potential energy curves associated with these axial perturbations (Figure 8, top panels) reveal that alterations to the Co−C bond length occur at a fairly steep energetic cost, particularly as the bond is shortened. In comparison, distortions along the Co−N_{ax} bonding coordinate are energetically less demanding, consistent with the axial bonding scheme described above. Lengthening of the Co−N_{ax} bond from its equilibrium position to 2.30 Å as observed in crystallographic studies (*14*) only requires ~2 kcal/mol and thus appears reasonable on the basis of energetic considerations. However, it is important to note that lengthening of this bond is associated with a shortening of the Co−C bond; thus, if anything, such an enzyme-induced elongation of the Co−N_{ax} bond would actually strengthen the Co−C bond of GM-bound CNCbl and, by analogy, AdoCbl.

These geometric/energetic relationships for CNCbl provide a fascinating complement to those established for MeCbl (*24*). In the case of MeCbl, the strongly σ-donating methyl group completely dominates the axial bonding scheme, inducing a sizable σ-antibonding interaction between the Co ion and the lower axial ligand, considerably weaken the Co−N_{ax} bond. Consequently, compared to CNCbl, distortions along the Co−N_{ax} bond of MeCbl define an even shallower potential energy surface and lead to minimal changes in the Co−C bond length. Collectively, our calculations for CNCbl and MeCbl thus provide a detailed understanding of how changes in the σ-donating ability of the upper axial ligand affect the axial bonding scheme and corroborate nicely with our qualitative model developed previously to rationalize trends in the axial bonding properties of Co^{3+}Cbl species (*33*).

To assess the spectroscopic consequences of the structural variations examined in Figure 8, TD-DFT was used to calculate the Abs spectrum for each CNCbl model considered. A subset of these spectra are presented in Figures 9

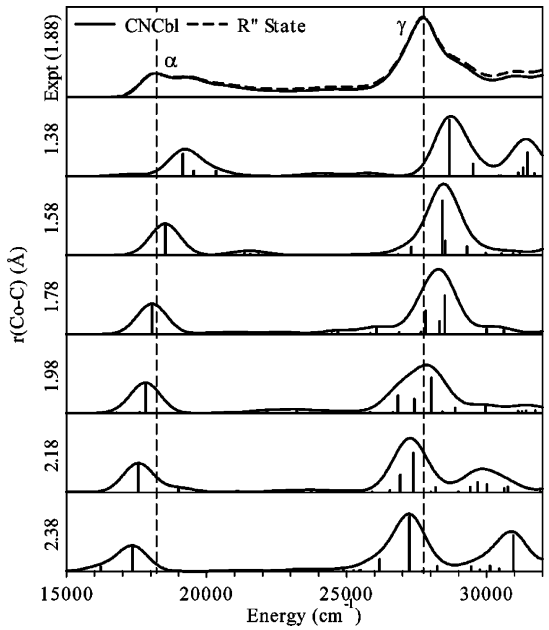

FIGURE 9: Representative TD-DFT-computed Abs spectra for CNCbl models, for which the upper axial Co−C bond length was systematically varied from 1.38 to 2.38 Å. Relevant structural parameters for these hypothetical models are given in Figure 7 and Table S25 in the Supporting Information. The experimental CNCbl and GM-bound CNCbl (R" state) Abs spectra are provided in the top panel for comparison.

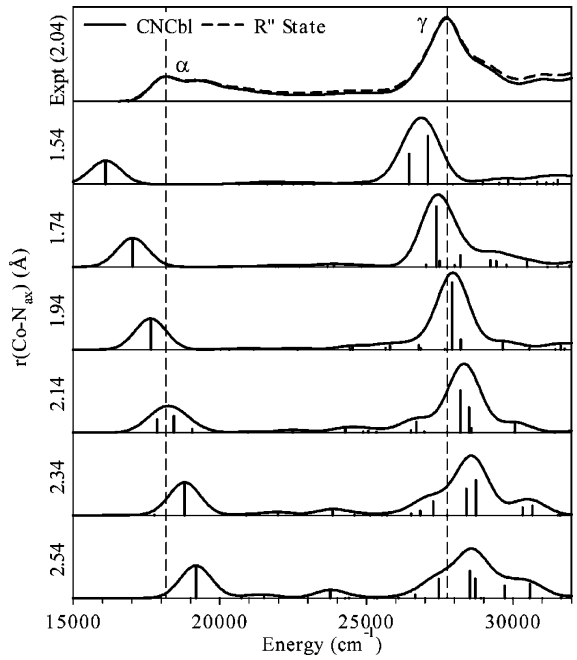

FIGURE 10: Representative TD-DFT-computed Abs spectra for CNCbl models, for which the lower axial Co−N_{ax} bond length was systematically varied from 1.54 to 2.54 Å. Relevant structural parameters for these hypothetical models are given in Figure 7 and Table S25 in the Supporting Information. The experimental CNCbl and GM-bound CNCbl (R″ state) Abs spectra are provided in the top panel for comparison.

and 10 (see Figures S4 and S5 in the Supporting Information for complete results) along with the experimental free CNCbl and R″ state Abs spectra. An examination of the computed spectra as a function of Co−C bond distortions reveals a consistent red shift of both the α band and the γ band. Within ±0.2 Å of the equilibrium Co−C bond length of 1.88 Å, the α band shifts ∼ −15 cm^{-1}/pm and the γ band shifts ∼ −20 cm^{-1}/pm as this bond is stretched. An opposite trend is observed upon lengthening the Co−N_{ax} bond, with the α and γ band blue shifting ∼ +31 cm^{-1}/pm and ∼ +16 cm^{-1}/pm, respectively, near the equilibrium Co−N_{ax} bond length of 2.04 Å. The observed shifts in the α band are primarily due to perturbations to the HOMO that serves as the donor MO for this low-energy transition. Although dominated by intracorrin π bonding, the HOMO does contain 1.5% Co $3d_{z^2}$ orbital character. Lengthening the Co−C bond mitigates the Co−C σ-bonding interaction and thus destabilizes the HOMO, reducing the HOMO−LUMO gap and red-shifting the α-band transition. Alternatively, lengthening of the Co−N_{ax} bond mitigates the Co−N_{ax} σ-antibonding interaction, stabilizing the HOMO and blue-shifting the transition. Interestingly, the lower σ-donor strength of CN^- relative to CH_3^- results in a significantly reduced Co $3d_{z^2}$ orbital contribution to the HOMO (only 1.5% Co $3d_{z^2}$ character for CNCbl as compared to 6% for MeCbl) and manifests itself in the smaller shifts predicted for the α band of CNCbl; i.e., for MeCbl, lengthening the Co−C and Co−N_{ax} bonds causes the α band to shift by ∼ −65 cm^{-1}/pm and ∼ +55 cm^{-1}/pm, respectively (*24*). Nevertheless, the fact that our calculations for CNCbl still predict sizable band shifts in response to axial bond distortions suggests that any changes to the axial bonding scheme upon incorporation of this cofactor into the GM active site should cause notable band shifts in the experimental spectra. Because no such band shifts are actually observed, we can conclude that the GM active site does not perturb the axial bonding interactions of CNCbl to any significant degree. In particular, our spectroscopic data do not support the existence of an unusually long Co−N_{ax} bond for CNCbl in the enzyme.

Co^{2+}Cbl Spectroscopy and Spectral Analysis. All Abs, CD, and MCD spectra obtained for samples containing Co^{2+}Cbl generated either through photolysis or under turnover conditions contained a mixture of Co^{3+}Cbl and Co^{2+}Cbl. Because both species exhibit similarly intense Abs and CD features, it was often difficult to discern contributions to the spectra arising solely from the Co^{2+}Cbl species. Fortunately, at low temperatures, the MCD technique is particularly sensitive to the paramagnetic Co^{2+}Cbl state of the cofactor, with the signal intensity at 4 K being nearly 10-fold greater for Co^{2+}-Cbl than for diamagnetic Co^{3+}Cbl. Thus, even for samples containing a mixture of Co^{3+}Cbl and Co^{2+}Cbl, MCD spectroscopy offers a direct probe of the Co^{2+}Cbl electronic structure. To ensure that differences between Co^{2+}Cbl spectra were not simply artifacts of the residual Co^{3+}Cbl signal, each Abs spectrum was fit to estimate the percent contributions from the two species and a corresponding fraction of the pure Co^{3+}Cbl MCD spectrum was then subtracted from the MCD spectrum of the Co^{2+}Cbl/Co^{3+}Cbl mixture. The resulting difference spectra were rescaled to match the signal intensity of the dominant feature at 30 300 cm^{-1} in the MCD spectrum of free Co^{2+}Cbl (Figure 11).

Free Co^{2+}Cbl. A detailed analysis of the Abs and MCD spectra of free Co^{2+}Cbl has been presented previously by our laboratory (*22*, *23*); the general band classifications established in these studies are provided in Figure 11. Low-energy bands arise primarily from ligand field (LF) transitions, with the lowest two bands ascribed to transitions from the Co $3d_{xz}$- and $3d_{yz}$-based MOs to the $3d_{z^2}$-derived MO.

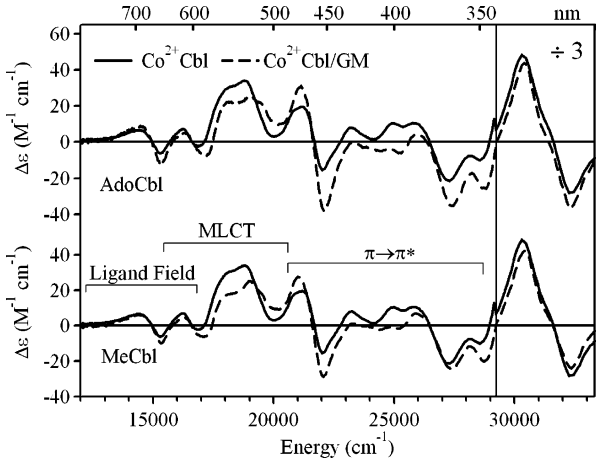

FIGURE 11: Comparison of the 4.5 K 7 T MCD spectra of free and GM-bound Co^{2+}Cbl generated through photolysis of the R state (top) and R′ state (bottom). Band classifications for free Co^{2+}Cbl are given in the lower panel.

The transitions giving rise to the bands between 16 000 and 20 500 cm^{-1} possess considerable Co 3d → corrin π^* metal-to-ligand charge transfer (MLCT) character, while the features between 20 500 and 29 000 cm^{-1} originate from ligand-centered transitions involving MOs of the corrin π system. The origin of the extremely intense derivative feature centered at 31 000 cm^{-1} is less well-understood, but the corresponding pair of transitions is thought to contain significant contributions from both corrin-centered and LF excitations. In all spectra presented herein, this spectral feature is scaled by a factor of one-third to facilitate a comparison of the less intense bands at lower energy.

Photolyzed Holo-GM. To assess whether and how the GM active site modulates the electronic properties of the Co^{2+}-Cbl form of the cofactor, MCD spectra were collected for photolyzed AdoCbl/GM and MeCbl/GM samples. In Figure 11, these spectra are overlaid with that of free Co^{2+}Cbl. Because of the significant contributions of the residual Co^{3+}-Cbl to the corresponding Abs and CD spectra, which prevented simultaneous Gaussian deconvolutions of these spectra and the MCD spectra (that are dominated by the Co^{2+}Cbl signal), only a qualitative analysis of the GM-bound Co^{2+}Cbl MCD spectra was carried out.

The photolyzed apo-GM samples reconstituted with AdoCbl and MeCbl yielded nearly identical MCD spectra (Figure 11), suggesting that the electronic structure of Co^{2+}Cbl in the GM active site is the same regardless of the identity of the upper axial ligand initially present. This similarity is not unexpected because the Co^{2+}Cbl photoproducts generated through photolysis of AdoCbl and MeCbl are, of course, identical. However, it does suggest that the presence of the bulky adenosyl moiety, which presumably resides in a binding pocket near the cofactor, does not appear to be necessary for the GM active site to perturb the Co^{2+}Cbl electronic structure.

Differences between the MCD spectra for the photolyzed holoenzyme samples and free Co^{2+}Cbl are particularly evident between 17 000 and 22 000 cm^{-1}. In this energy range, several bands in the photolyzed R/R′ state spectra are blue-shifted slightly relative to those in the spectrum of the unbound cofactor and the derivative-shaped feature centered around 21 000 cm^{-1} shows a significant gain in intensity.

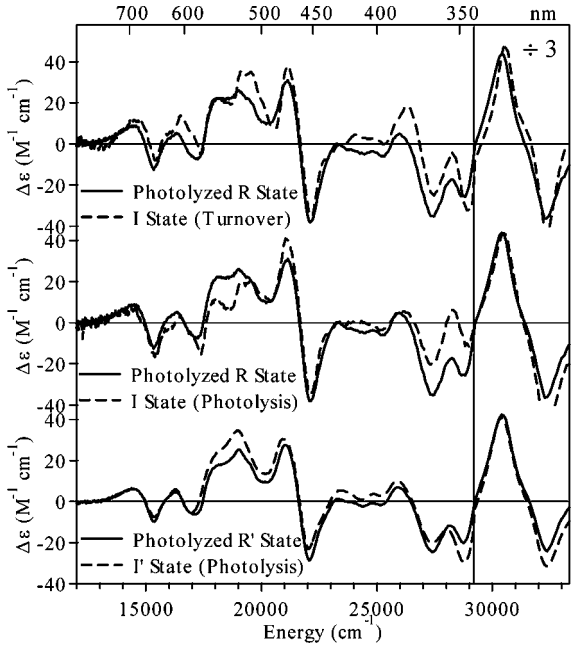

FIGURE 12: Comparison of the 4.5 K 7 T MCD spectra of the photolyzed R/R′ states and the corresponding I/I′ states obtained either via the addition of glutamate (top) or through photolysis of substrate-bound GM reconstituted with AdoCbl (center) and MeCbl (bottom).

Interestingly, however, a number of other features peak at nearly the same energy in all three spectra presented in Figure 11. These features include the two lowest energy bands, the derivative-shaped feature centered at 21 600 cm^{-1}, and the intense derivative-shaped feature centered at 30 300 cm^{-1}. On the basis of our previous electronic structure analysis of free Co^{2+}Cbl, the features most affected by cofactor binding to the GM active site possess considerable MLCT character, while the LF and corrin-centered $\pi \rightarrow \pi^*$ transitions to lower and higher energies, respectively, are insignificantly perturbed. Overall, these results reveal that the protein alters the electronic structure of the Co^{2+}Cbl form of the cofactor to a small but significant extent even in the absence of substrate, modulating the energy difference between the Co 3d-based and corrin π/π^*-based MOs.

Intermediate (I) State. As noted above, holo-GM reconstituted with AdoCbl was observed to generate a sizable amount of Co^{2+}Cbl upon the addition of substrate or any of the substrate analogues. Although Co^{2+}Cbl only accounted for ~15% of the total Cbl present in each sample (on the basis of an analysis of the corresponding Abs spectra), at low temperatures the MCD spectrum is dominated by contributions from this paramagnetic species, thus allowing for the detection of an essentially pure I state spectrum. All of the substrate analogues used yielded I state MCD spectra nearly identical to those obtained using the native substrate glutamate; a comparison of these data sets is provided in the Supporting Information (Figure S6). A representative example of the richly structured MCD spectrum of the I state generated by the addition of glutamate to holo-GM is shown in Figure 12 (top) along with that of Co^{2+}Cbl/GM generated through photolysis of AdoCbl/GM. While the overall appearance of the two spectra is very similar, several bands in the I state spectrum are shifted to the blue, particularly those between 16 000 and 18 000 cm^{-1} and between 29 000 and 31 000 cm^{-1}, and a prominent double-peaked feature appears

near 19 500 cm^{-1}. Interestingly, all of these spectral alterations involve transitions possessing significant MLCT character. In contrast, the LF and corrin-centered transitions of GM-bound Co^{2+}Cbl are largely unaffected by the presence of glutamate in the enzyme active site, suggesting that activation of the Co−C bond may involve enzymatic stabilization of the Co 3d orbitals.

In an attempt to increase the percentage of Co^{2+}Cbl in the I state samples, each of the substrate (analogue)-bound samples described above was subjected to photolysis (see the Materials and Methods section). On the basis of an analysis of the corresponding Abs spectra, the photolyzed samples were estimated to contain between 15% (for 2-methyleneglutarate) and 35% (for 2-hydroxyglutarate) Co^{2+}Cbl. In Figure 12 (center), the MCD spectrum of the photolyzed I state sample generated by the addition of glutamate to holo-GM is overlaid with that of the photolyzed AdoCbl/GM sample. As noted above for the MCD spectrum of the I state generated by catalytic turnover (Figure 12, top), several bands in the photolyzed I state spectrum are blue-shifted with respect to their counterparts in the photolyzed AdoCbl/GM MCD spectrum. The unique double-peaked feature again appears near 19 500 cm^{-1}, although in this case it carries less intensity relative to the remainder of the spectrum. However, while the catalytically generated I state samples all exhibit nearly identical MCD spectra (as described in the preceding paragraph), photolysis of these samples does not result in the appearance of equivalent MCD spectra. Instead, while the MCD spectra of glutamate- and 2-methyleneglutarate-containing samples closely resemble those of the corresponding catalytic I state MCD spectra, the MCD spectra of samples containing 2-hydroxyglutarate and 3-methylaspartate are strikingly more similar to the photolyzed holoenzyme spectrum and notably lack the double-peaked feature at 19 500 cm^{-1} (Figure S7 in the Supporting Information). Interestingly, photolysis of the glutamate- and 2-methyleneglutarate-containing I state samples resulted in minimal increases in the percent of Co^{2+}Cbl in the sample mixture (to 15 and 20%, respectively), whereas the percentage of Co^{2+}Cbl in the 2-hydroxyglutarate- and 3-methylaspartate-containing I state samples increased significantly (to 35 and 33%, respectively). Thus, any significant increase in the percentage of AdoCbl → Co^{2+}Cbl conversion through photolysis appears to be due to formation of a Co^{2+}-Cbl species that is not representative of the catalytic I state. An inactive form of the I state has been observed previously by EPR spectroscopy for substrate-bound samples incubated overnight (*15*, *63*). On the basis of the similarity between the inactive I state MCD spectra and that of the photolyzed R state, this new paramagnetic species appears to have lost the substrate from the GM active site. Loss of the slow substrate analogue 2-hydroxyglutarate from the active site is not unexpected considering its relatively large K_d value of 3 mM (*29*) and the fact that substrate binding and release rates are fast relative to turnover (*64*).

Complementary photolysis experiments were performed on the substrate (analogue)-bound MeCbl/GM samples (S′/P′ states) to generate the corresponding I′ state. These photolyzed samples did not exhibit MCD signals similar to the I state but instead displayed MCD spectra reminiscent of the photolyzed R′ state spectrum (Figure 12, bottom). Regardless of the substrate (analogue) present in the I′ state, an MCD spectrum similar to that shown in Figure 12 (bottom) was obtained except when glutamate was used, in which case a moderately different MCD spectrum resulted (Figure S8 in the Supporting Information) that resembles previously published MCD spectra of Co^{2+}Cbi (*23*), where the lower axial base is replaced by a H_2O molecule. The inability of these photolyzed MeCbl substrate state samples to generate the characteristic I state MCD spectral features, in particular the double-peaked feature at 19 500 cm^{-1}, suggests that the adenosyl moiety plays an essential role in organizing the GM active site for stabilization of the post-homolysis product Co^{2+}Cbl.

DISCUSSION

While the mechanistic role of the Cbl cofactor in B_{12}-dependent isomerases was established years ago (*65*, *66*), detailed electronic structure descriptions of the enzyme-bound cofactor in both the Co^{3+}Cbl ground state and the post-homolysis Co^{2+}Cbl state have been lacking. In this study, we have employed a combination of spectroscopic and computational tools to examine the enzyme/cofactor interactions in GM following an approach similar to that recently applied to the Cbl-dependent enzyme MMCM (*22*, *24*). Using several complementary spectroscopic techniques to evaluate changes in the electronic structure of the enzyme/cofactor complexes in the absence and presence of substrate (or a substrate analogue), we were able to evaluate the relative importance of the two potential Co−C bond activation mechanisms outlined in the Introduction. Below, we combine insights gained in these studies with those from our previous investigations of MMCM to evaluate possible mechanisms by which the enzyme/cofactor interactions may serve to activate the Co−C bond for homolytic cleavage as the first step in the unique rearrangement reactions catalyzed by Cbl-dependent isomerases.

Ground-State Destabilization. One of the two possible routes by which GM could instigate the trillion-fold rate increase in homolytic Co−C bond cleavage of AdoCbl is through destabilization of the Co^{3+}Cbl "ground state". The 10^{12}-fold rate enhancement observed for homolytic cleavage of the cofactor's Co−C bond when bound to GM would likely manifest itself in a dramatic alteration of the Co−C bonding scheme and, on the basis of previous electronic structure studies of Co^{3+}Cbls, be revealed through substantial changes in the electronic spectroscopy of the cofactor. For example, although the lowest energy transition observed in the Abs, CD, and MCD spectra of AdoCbl (the α band) involves excitation of an electron from the largely corrin π-based HOMO to the corrin π^*-based LUMO, the HOMO also contains ∼6% Co $3d_{z^2}$-orbital character. Similar contributions to the HOMO from the Co $3d_{z^2}$ orbital are predicted for MeCbl (∼6%) and CNCbl (∼1.5%). On the basis of the spectro/structural correlations developed for MeCbl (*24*) and CNCbl (this paper), lengthening of the Co−C bond (and consequent weakening of this bonding interaction) is predicted to red-shift the α band by −65 pm/Å and −15 pm/Å, respectively. However, the spectroscopic studies presented here for holo-GM in the absence and presence of substrate analogues do not indicate any significant alterations in the position of the α-band transition. These results agree well with previous rR studies that revealed a frequency shift of less than 2 cm^{-1} for the Co−C stretching mode of holo-GM

as compared to free AdoCbl, implying that the cofactor's Co−C bond is not weakened in the enzyme active site (*19*). Collectively, the wealth of spectroscopic data available to date provides compelling evidence that GM does not activate the Co−C bond of the Co^{3+}Cbl cofactor to any significant extent even in the presence of substrate (or a substrate analogue).

Our spectroscopic data, along with our spectro/structural correlations, also provide insight into the significance of the cofactor's lower axial ligand switch and the existence of an unusually long Co−N_{ax} bond in GM seemingly observed by X-ray crystallography. Interestingly, the DMB → His ligand switch accompanying cofactor binding to apo-GM does not appear to influence the electronic structure of the cofactor to any noticeable degree in the ground state, as revealed by the close resemblance of the electronic spectra obtained for the free and GM-bound Co^{3+}Cbl cofactors. The lack of any major spectral changes also refutes the existence of a "long" Co−N_{ax} bond observed in earlier crystallographic studies [∼2.35 Å for MeCbl and ∼2.30 Å for CNCbl (*14*)], because our spectro/structural correlations for MeCbl and CNCbl indicate that the α-band transition would blue-shift by ∼ +55 cm^{-1}/pm and ∼ +31 cm^{-1}/pm, respectively, in response to changes in this structural coordinate. Consequently, an increase in the Co−N_{ax} bond length of MeCbl and CNCbl from their equilibrium distances of 2.16 and 2.04 Å, respectively, to the values reported for the GM-bound cofactors would result in blue shifts of the α-band transition by ∼1050 and ∼800 cm^{-1}, respectively. Because changes of these magnitudes are not observed for the holo-GM spectra in the absence or presence of substrate (or a substrate analogue), our data are consistent with EXAFS studies by Champloy et al. (*17*) and more recent X-ray structural results (*18*), supporting the conclusion that the long Co−N_{ax} bond lengths observed in the earlier X-ray structures were mere artifacts. Thus, despite the intriguing ligand switch at the lower axial coordination site, the change in the identity of the axial base does not appear to provide a mechanism by which GM activates the cofactor in the ground state for homolytic Co−C bond cleavage.

Stabilization of the Post-Homolysis Product Co^{2+}Cbl. While few significant changes are observed in the electronic spectra of the Co^{3+}Cbl/GM complexes, notable differences exist between the MCD spectra of GM-bound and free Co^{2+}-Cbl. Interestingly, formation of Co^{2+}Cbl in the GM active site in the presence of substrate (or a substrate analogue) via catalytic turnover leads to even greater perturbations of the electronic structure of the Co^{2+}Cbl cofactor, as evidenced by further changes to the MCD spectrum. Analysis of these data within the theoretical framework established previously (*22*) reveals that the features of the Co^{2+}Cbl MCD spectrum most strongly altered by incorporation of the cofactor into the GM active site primarily arise from MLCT transitions. Specifically, while the transitions formally corresponding to LF and corrin $\pi \rightarrow \pi^*$ excitations exhibit negligible changes in energy, most of the MLCT transitions display a considerable blue shift and, in the case of the catalytically formed I state complexes, a unique double-peaked feature appears in the MCD spectrum at 19 500 cm^{-1}. One way in which the energies of the MLCT transitions but not the LF and corrin $\pi \rightarrow \pi^*$ transitions could be affected is through a uniform stabilization of the Co 3d-based MOs. In this case, the energy gap between the metal 3d- and corrin π^*-based MOs would increase without considerably affecting the energy separation between the corrin π- and π^*-based MOs or the LF splitting of the Co^{2+} 3d orbitals.

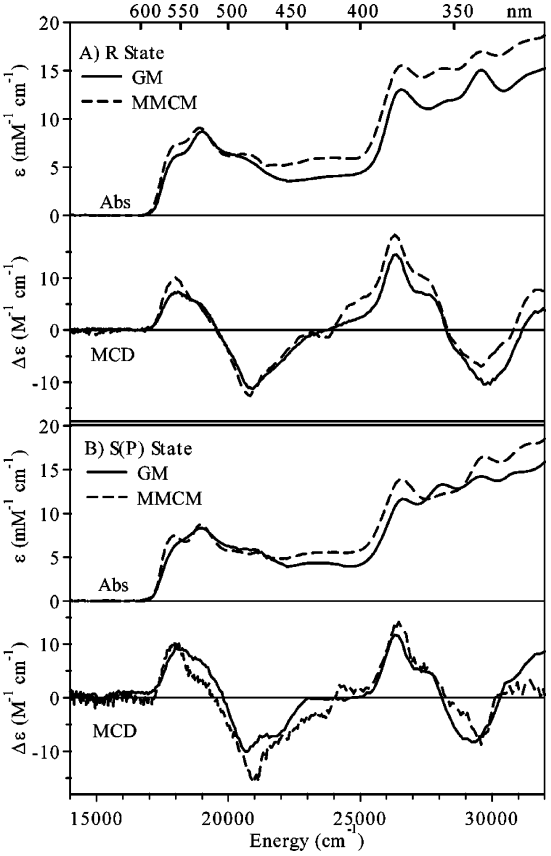

FIGURE 13: Comparison of the 4.5 K Abs and 25 K 7 T MCD spectra of (A) the R states and (B) the S(P) states of GM and MMCM.

Comparisons to MMCM. MMCM is a second member of the AdoCbl-dependent carbon skeleton isomerase subfamily whose global fold bears a remarkable resemblance to that of GM (*1*, *14*, *18*, *67*), suggesting that the two enzymes are designed to interact with the Cbl cofactors in a similar manner. In the Co^{3+}Cbl ground state, this hypothesis is supported by the similarity of the holo-GM and holo-MMCM Abs and MCD spectra in the absence and presence of substrate (or a substrate analogue) (Figure 13), with both enzymes inducing only minor changes to the electronic structure of the cofactor. Qualitatively, the only noticeable difference between the GM and MMCM spectra is the increased Abs intensity at higher energy for the R state of MMCM as compared to that of GM (Figure 13A). Because the Abs intensity in this region is known to correlate with the dielectric constant of the cofactor environment (*58*), this difference can be attributed to the fact that the GM active site lies at the interface of two subunits, rendering it more solvent-exposed than the MMCM active site, which is buried inside a single subunit. More importantly, however, neither the R state nor the S state spectra for both GM (this paper) and MMCM (*24*) display any significant band shifts compared to the free AdoCbl spectra. As such, it is reasonable to conclude that neither enzyme promotes Co−C bond homolysis through destabilization of the Co^{3+}Cbl ground state.

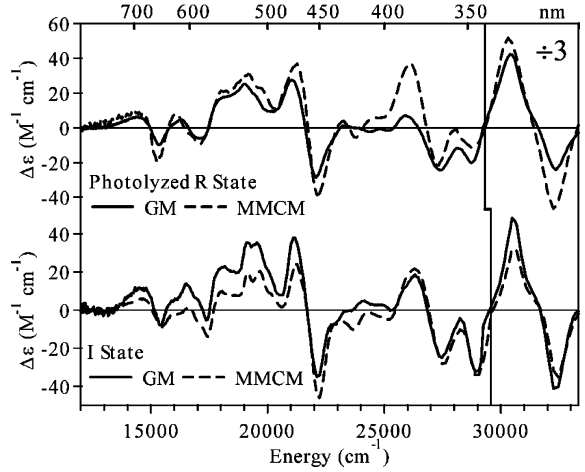

FIGURE 14: Comparison of the 4.5 K 7 T MCD spectra of the photolyzed R state (top) and the I state (bottom) for GM (—) and MMCM (- - -).

Our spectroscopic data demonstrate that GM alters the electronic structure of the Co^{2+}Cbl state of the bound cofactor in both the absence and presence of substrate (or a substrate analogue). Interestingly, the photolyzed R state and I state spectra for GM are almost identical to the corresponding spectra obtained for MMCM (Figure 14). The ability of both enzymes to alter the electronic structure of the Co^{2+}Cbl cofactor in the same manner and to the same extent implies that a common mechanism is being employed to perturb the post-homolysis Cbl product. On the basis of the observation that MMCM primarily perturbs the MLCT transitions of Co^{2+}Cbl, a mechanism was proposed invoking a uniform stabilization of the cobalt 3d orbitals through reduction of the charge donation from the axial ligand to the cobalt center (*22*). Although the lower axial ligand switch upon formation of the holoenzyme is not observed to alter the electronic structure of the ground-state complexes, it is possible that the His residue may play an important role in stabilizing the Co^{2+}Cbl form of the cofactor.[7] Because of the similarity of the spectroscopic results presented above for GM to those reported for MMCM (*22*), we suggest that a similar mechanism of activation is operative in GM and may well extend to other members of the base-off Cbl-dependent isomerase family (*68*).

ACKNOWLEDGMENT

The authors thank Dr. Martin T. Zanni and Amber T. Krummel for use of and help with their FTIR spectrometer and Dr. Frank Neese (MPI Mülheim) for supplying a free copy of the ORCA software package.

SUPPORTING INFORMATION AVAILABLE

Cartesian coordinates for all CNCbl models generated by partial DFT geometry optimizations, additional Abs, CD, and MCD spectra of substrate (analogue) states not presented in the text, additional Gaussian deconvolution parameters not presented in the text, FT-IR spectra of free and GM-bound CNCbl, table of structural and energetic correlations derived from the CNCbl spectro/structural correlations, TD-DFT spectra for all optimized CNCbl models, and all I state MCD spectra for substrate (analogue)-bound AdoCbl/GM (generated catalytically and via photolysis) and MeCbl/GM (obtained via photolysis). This material is available free of charge via the Internet at http://pubs.acs.org.

[7] While the spectroscopic results obtained in this study conclusively demonstrate that the post-homolysis product Co^{2+}Cbl is significantly perturbed by the GM active site, no simple correlation exists between the observed MCD band shifts and the extent of enzymatic stabilization of the GM-bound reduced cofactor.

REFERENCES

1. Banerjee, R. (2003) Radical carbon skeleton rearrangements: Catalysis by coenzyme B_{12}-dependent mutases, *Chem. Rev. 103*, 2083−2094.
2. Frey, P. A. (2001) Radical mechanisms of enzymatic catalysis, *Annu. Rev. Biochem. 70*, 121−148.
3. Gruber, K., and Kratky, C. (2002) Coenzyme B_{12} dependent glutamate mutase, *Curr. Opin. Chem. Biol. 6*, 598−603.
4. Marsh, E. N. G. (2000) Coenzyme B_{12}-dependent glutamate mutase, *Bioorg. Chem. 28*, 176−189.
5. Marsh, E. N. G., and Drennan, C. L. (2001) Adenosylcobalamin-dependent isomerases: New insights into structure and mechanism, *Curr. Opin. Chem. Biol. 5*, 499−505.
6. Toraya, T. (2003) Radical catalysis in coenzyme B_{12}-dependent isomerization (eliminating) reactions, *Chem. Rev. 103*, 2095−2127.
7. Barker, H. A., Rooze, V., Suzuki, F., and Iodice, A. A. (1964) The glutamate mutase system, *J. Biol. Chem. 239*, 3260−3266.
8. Chih, H. W., and Marsh, E. N. G. (2000) Mechanism of glutamate mutase: Identification and kinetic competence of acrylate and glycyl radical as intermediates in the rearrangement of glutamate to methylaspartate, *J. Am. Chem. Soc. 122*, 10732−10733.
9. Bothe, H., Darley, D. J., Albracht, S. P. J., Gerfen, G. J., Golding, B. T., and Buckel, W. (1998) Identification of the 4-glutamyl radical as an intermediate in the carbon skeleton rearrangement catalyzed by coenzyme B_{12}-dependent glutamate mutase from *Clostridium cochlearium*, *Biochemistry 37*, 4105−4113.
10. Buckel, W., and Golding, B. T. (1996) Glutamate and 2-methyleneglutarate mutase: From microbial curiosities to paradigms for coenzyme B_{12}-dependent enzymes, *Chem. Soc. Rev. 25*, 329−337.
11. Wetmore, S. D., Smith, D. M., Golding, B. T., and Radom, L. (2001) Interconversion of (*S*)-glutamate and (2*S*,3*S*)-3-methylaspartate: A distinctive B_{12}-dependent carbon-skeleton rearrangement, *J. Am. Chem. Soc. 23*, 7963−7972.
12. Hay, B. P., and Finke, R. G. (1986) Thermolysis of the Co−C bond of adenosylcobalamin. 2. Products, kinetics, and Co−C bond dissociation energy in aqueous solution, *J. Am. Chem. Soc. 108*, 4820−4829.
13. Marsh, E. N. G., and Ballou, D. P. (1998) Coupling of cobalt−carbon bond homolysis and hydrogen atom abstraction in adenosylcobalamin-dependent glutamate mutase, *Biochemistry 37*, 11864−11872.
14. Reitzer, R., Gruber, K., Jogl, G., Wagner, U. G., Bothe, H., Buckel, W., and Kratky, C. (1999) Glutamate mutase from *Clostridium cochlearium*: The structure of a coenzyme B_{12}-dependent enzyme provides new mechanistic insights, *Struct. Fold. Des. 7*, 891−902.
15. Zelder, O., Beatrix, B., Kroll, F., and Buckel, W. (1995) Coordination of a histidine residue of the protein-component S to the cobalt atom in coenzyme B_{12}-dependent glutamate mutase from *Clostridium cochlearium*, *FEBS Lett. 369*, 252−254.
16. De Ridder, D. J. A., Zangrando, E., and Bürgi, H. B. (1996) Structural behaviour of cobaloximes: Planarity, an anomalous trans-influence and possible implications on Co−C bond cleavage in coenzyme-B_{12}-dependent enzymes, *J. Mol. Struct. 374*, 63−83.
17. Champloy, F., Jogl, G., Reitzer, R., Buckel, W., Bothe, H., Beatrix, B., Broeker, G., Michalowicz, A., Meyer-Klaucke, W., and Kratky, C. (1999) EXAFS data indicate a "normal" axial cobalt−nitrogen bond of the organo-B_{12} cofactor in the two coenzyme B_{12}-dependent enzymes glutamate mutase and 2-methyleneglutarate mutase, *J. Am. Chem. Soc. 121*, 11780−11789.
18. Gruber, K., Reitzer, R., and Kratky, C. (2001) Radical shuttling in a protein: Ribose pseudorotation controls alkyl-radical transfer in the coenzyme B_{12} dependent enzyme glutamate mutase, *Angew. Chem. Int. Ed. 40*, 3377−3380.

19. Huhta, M. S., Chen, H.-P., Hemann, C., Hille, C. R., and Marsh, E. N. G. (2001) Protein−coenzyme interactions in adenosylcobalamin-dependent glutamate mutase, *Biochem. J. 355*, 131−137.
20. Licht, S., Booker, S., and Stubbe, J. (1999) Studies on the catalysis of carbon−cobalt bond homolysis by ribonucleoside triphosphate reductase: Evidence for concerted carbon−cobalt bond homolysis and thiyl radical formation, *Biochemistry 38*, 1221−1233.
21. Chowdhury, S., and Banerjee, R. (2000) Thermodynamic and kinetic characterization of Co−C bond homolysis catalyzed by coenzyme B_{12}-dependent methylmalonyl-CoA mutase, *Biochemistry 39*, 7998−8006.
22. Brooks, A. J., Vlasie, M., Banerjee, R., and Brunold, T. C. (2005) Co−C bond activation in methylmalonyl-CoA mutase by stabilization of the post-homolysis product Co^{2+}cobalamin, *J. Am. Chem. Soc.*, manuscript submitted.
23. Stich, T. A., Buan, N. R., and Brunold, T. C. (2004) Spectroscopic and computational studies of Co^{2+}corrinoids: Spectral and electronic properties of the biologically relevant base-on and base-off forms of Co^{2+}cobalamin, *J. Am. Chem. Soc. 126*, 9735−9749.
24. Brooks, A. J., Vlasie, M., Banerjee, R., and Brunold, T. C. (2004) Spectroscopic and computational studies on the adenosylcobalamin-dependent methylmalonyl-CoA mutase: Evaluation of enzymatic contributions to Co−C bond activation in the Co^{3+} ground state, *J. Am. Chem. Soc. 126*, 8167−8180.
25. Hartrampf, G., and Buckel, W. (1986) On the steric course of the adenosylcobalamin-dependent 2-methyleneglutarate mutase reaction in clostridium-barkeri, *Eur. J. Biochem. 156*, 301−304.
26. Fonseca, M. V., and Escalante-Semerena, J. C. (2000) Reduction of cob(III)alamin to cob(II)alamin in *Salmonella enterica* serovar typhimurium LT2, *J. Bacteriol. 182*, 4304−4309.
27. Fonseca, M. V., and Escalante-Semerena, J. C. (2001) An *in vitro* reducing system for the enzymic conversion of cobalamin to adenosylcobalamin, *J. Biol. Chem. 276*, 32101−32108.
28. Chen, H. P., and Marsh, E. N. G. (1997) Adenosylcobalamin-dependent glutamate mutase: Examination of substrate and coenzyme binding in an engineered fusion protein possessing simplified subunit structure and kinetic properties, *Biochemistry 36*, 14939−14945.
29. Cheng, M.-C. Mechanistic studies of adenosylcobalamin homolysis in glutamate mutase, Ph.D. Thesis, University of Michigan, Ann Arbor, MI, 2004.
30. Roymoulik, I., Moon, N., Dunham, W. R., Ballou, D. P., and Marsh, E. N. G. (2000) Rearrangement of L-2-hydroxyglutarate to L-*threo*-3-methylmalate catalyzed by adenosylcobalamin-dependent glutamate mutase, *Biochemistry 39*, 10340−10346.
31. Schneider, Z., and Stroinski, A. (1987) *Comprehensive B_{12}: Chemistry, Biochemistry, Nutrition, Ecology, and Medicine*, De Gruyter, New York.
32. Randaccio, L., Furlan, M., Geremia, S., Slouf, M., Srnova, I., and Toffoli, D. (2000) Similarities and differences between cobalamins and cobaloximes. Accurate structural determination of methylcobalamin and of LiCl- and KCl-containing cyanocobalamins by synchrotron radiation, *Inorg. Chem. 39*, 3403−3413.
33. Stich, T. A., Brooks, A. J., Buan, N. R., and Brunold, T. C. (2003) Spectroscopic and computational studies of Co^{3+}-corrinoids: Spectral and electronic properties of the B_{12} cofactors and biologically relevant precursors, *J. Am. Chem. Soc. 125*, 5897−5914.
34. Jensen, K. P., and Ryde, U. (2002) The axial N-base has minor influence on the Co−C bond cleavage in cobalamins, *Theochem 585*, 239−255.
35. Rovira, C., Biarnés, X., and Kunc, K. (2004) Structure-energy relations in methylcobalamin with and without bound axial base, *Inorg. Chem. 43*, 6628−6632.
36. Guerra, C. F., Snijders, J. G., te Velde, G., and Baerends, E. J. (1998) Towards an order-N DFT method, *Theor. Chem. Acc. 99*, 391−403.
37. te Velde, G., Bickelhaupt, F. M., van Gisbergen, S. J. A., Guerra, C. F., Baerends, E. J., Snijders, J. G., and Ziegler, T. (2001) Chemistry with ADF, *J. Comput. Chem. 22*, 931−967.
38. ADF2002.03, SCM, Theoretical Chemistry, Vrije Universiteit, Amsterdam, The Netherlands, http://www.scm.com.
39. Vosko, S. H., Wilk, L., and Nusair, M. (1980) Accurate spin-dependent electron liquid correlation energies for local spin density calculations: A critical analysis, *Can. J. Phys. 58*, 1200−1211.
40. Becke, A. D. (1986) Density functional calculations of molecular bond energies, *J. Chem. Phys. 84*, 4524−4529.
41. Perdew, J. P. (1986) Density functional approximation for the correlation energy of the inhomogeneous electron gas, *Phys. Rev. B 33*, 8822−8824.
42. Neese, F. *ORCA*, version 2.2, an ab initio, density functional, and semiempirical program package, Max-Planck-Institut für Bioanorganische Chemie: Mülheim an der Ruhr, Germany, 2001.
43. Ahlrichs, R., and co-workers, unpublished results.
44. Schäfer, A., Horn, H., and Ahlrichs, R. (1992) Fully optimized contracted Gaussian-basis sets for atoms Li to Kr, *J. Chem. Phys. 97*, 2571−2577.
45. The Ahlrichs auxiliary basis sets were obtained from the TurboMole basis set library under ftp.chemie.uni-karlsruhe.de/pub/cbasen. Weigend, F., and Häser, M. (1997) RI-MP2: First derivatives and global consistency, *Theor. Chem. Acc. 97*, 331−340.
46. Schäfer, A., Huber, C., and Ahlrichs, R. (1994) Fully optimized contracted Gaussian-basis sets of triple ζ valence quality for atoms Li to Kr, *J. Chem. Phys. 100*, 5829−5835.
47. Becke, A. D. (1993) Density-functional thermochemistry. 3. The role of exact exchange, *J. Chem. Phys. 98*, 5648−5652.
48. Becke, A. D. (1993) A new mixing of Hartree−Fock and local density-functional theories, *J. Chem. Phys. 98*, 1372−1377.
49. Lee, C. T., Yang, W. T., and Parr, R. G. (1988) Development of the Colle−Salvetti correlation-energy formula into a functional of the electron density, *Phys. Rev. B 37*, 785−789.
50. Bauernschmitt, R., and Ahlrichs, R. (1996) TD-DFT, *Chem. Phys. Lett. 256*, 454−464.
51. Casida, M. E., Jamorski, C., Casida, K. C., and Salahub, D. R. (1998) Molecular excitation energies to high-lying bound states from time-dependent density-functional response theory: Characterization and correction of the time-dependent local density approximation ionization threshold, *J. Chem. Phys. 108*, 4439−4449.
52. Stratman, R. E., Scuseria, G. E., and Frisch, M. J. (1998) An efficient implementation of time-dependent density-functional theory for the calculation of excitation energies of large molecules, *J. Chem. Phys. 109*, 8218−8224.
53. Hirata, S., and Head-Gordon, M. (1999) Time-dependent density functional theory for radicals−An improved description of excited states with substantial double excitation character, *Chem. Phys. Lett. 302*, 375−382.
54. Hirata, S., and Head-Gordon, M. (1999) Time-dependent density functional theory within the Tamm−Dancoff approximation, *Chem. Phys. Lett. 314*, 291−299.
55. Neese, F., and Olbrich, G. (2002) Efficient use of the resolution of the identity approximation in time-dependent density functional calculations with hybrid density functionals, *Chem. Phys. Lett. 362*, 170−178.
56. Andruniow, T., Kozlowski, P. M., and Zgierski, M. Z. (2001) Theoretical analysis of electronic absorption spectra of vitamin B_{12} models, *J. Chem. Phys. 115*, 7522−7533.
57. Firth, R. A., Hill, H. A. O., Pratt, J. M., Williams, R. J. P., and Jackson, W. R. (1967) The circular dichroism and absorption spectra of some vitamin B_{12} derivatives, *Biochemistry 6*, 2178−2189.
58. Chowdhury, S., and Banerjee, R. (1999) Role of the dimethylbenzimidazole tail in the reaction catalyzed by coenzyme B_{12}-dependent methylmalonyl-CoA mutase, *Biochemistry 38*, 15287−15294.
59. Bax, A., Marzilli, L. G., and Summers, M. F. (1987) New insights into the solution behavior of cobalamins: Studies of the base-off form of coenzyme B_{12} using modern two-dimensional NMR methods, *J. Am. Chem. Soc. 109*, 566−574.
60. Marques, H. M., Zou, X., and Brown, K. L. (2000) The solution structure of adenosylcobalamin and adenosylcobinamide determined by NOE-restrained molecular dynamics simulations, *J. Mol. Struct. 520*, 75−95.
61. Marques, H. M., and Brown, K. L. (2002) Molecular mechanics and molecular dynamics simulations of porphyrins, metalloporphyrins, heme proteins, and cobalt corrinoids, *Coord. Chem. Rev. 225*, 123−158.
62. Galluzzi, F., Garozzo, M., and Ricci, F. F. (1974) Resonance Raman scattering and vibronic coupling in aquo- and cyanocobalamin, *J. Raman Spectrosc. 2*, 351−362.
63. Zelder, O., Beatrix, B., Leutbecher, U., and Buckel, W. (1994) Characterization of the coenzyme B_{12}-dependent glutamate mutase from *Clostridium cochlearium* produced in *Escherichia coli*, *Eur. J. Biochem. 226*, 577−585.

64. Chih, H. W., and Marsh, E. N. G. (1999) Pre-steady-state kinetic investigation of intermediates in the reaction catalyzed by adenosylcobalamin-dependent glutamate mutase, *Biochemistry 38*, 13684−13691.
65. Babior, B. M. (1975) Mechanism of cobalamin-dependent rearrangements, *Acc. Chem. Res. 8*, 376−384.
66. Halpern, J. (1985) Mechanisms of coenzyme B_{12}-dependent rearrangements, *Science 227*, 869−875.
67. Mancia, F., Smith, G. A., and Evans, P. R. (1999) Crystal structure of substrate complexes of methylmalonyl-CoA mutase, *Biochemistry 38*, 7999−8005.
68. While this paper was under review, a computational study of glutamate mutase was published in which the Co−C bond activation mechanism was examined using combined quantum mechanics/molecular mechanics methods: Jensen, K. P., and Ryde, U. (2005) How the Co−C bond is cleaved in coenzyme B_{12} enzymes: A theoretical study, *J. Am. Chem. Soc. 127*, 9117−9128. It was suggested that four terms contribute to the rate acceleration for Co−C bond cleavage by B_{12}-dependent enzymes: (i) the Ado· radical is kept within 4.2 Å of the Co ion (equivalent to a cage effect; a decrease in computed bond dissociation energy by 20 kJ/mol); (ii) the surrounding enzyme stabilizes the dissociated state via electrostatic and van der Waals interactions (42 kJ/mol); (iii) the protein is stabilized in the dissociated state (11 kJ/mol); and (iv) the protein preferentially distorts the cofactor in its Co^{3+}Cbl state (61 kJ/mol). We note, however, that, although this study was carried out thoughtfully and employed state-of-the-art computational methods, the geometric distortions predicted for the Co^{3+}Cbl ground state, with optimized Co−C and Co−N_{ax} bond lengths of 2.09 and 2.49 Å, respectively, are inconsistent with our spectroscopic data, suggesting that this state is poorly described computationally. Consequently, the accuracy of the computed contributions to the enzymatic reduction in bond dissociation energy is somewhat questionable.

BI051094Y